*Progress In Electromagnetics Research C, Vol. 123, 135–150, 2022*

# Fast Predictive Switching Table-Based Model Predictive Torque Control for PMSM

**Cheng Zhang[1, 2], Zichen Xiong[1], Yang Zhang[1, *], Hao Xie[1], and Pengcheng Zhang[1]**

**Abstract**—To reduce the calculation time of traditional model predictive torque control (MPTC), lower torque ripple, and improve the dynamic characteristics of predictive control, a model predictive torque control strategy applied in permanent magnet synchronous motor (PMSM) based on fast predictive switching table is proposed. This paper presents the 12-sector division method first. Then, based on sector division MPTC, a fast predictive switching table is proposed to reduce the 14 candidate voltage vectors of the sector division MPTC to 5. In addition, the the Proportional Integral (PI)-based adjustable weight coefficient is designed, so that the two physical quantities in the cost function have different weights under different working conditions, which improves the dynamic response of the system. As the experiment shows, PMSM uses the control strategy of this paper to output smaller torque steady-state fluctuation and faster dynamic response.

## 1. INTRODUCTION

In recent years, Model Predictive Control (MPC) has been continuously studied and applied in the field of PMSM control [1, 2]. Compared with Vector Control (VC) [3] and Direct Torque Control (DTC) [4], MPC system intuitively expresses the future state of variables, optimizes the output, and has better dynamic response characteristics [5]. The rotational speed predictive control is more dependent on the motor parameters. There are heavy workloads, a large feedback delay, and many parameters that need to be adjusted in the design. It has poor anti-interference and robustness [6, 7]. Therefore, model predictive control is more used in current or torque control [8, 9], where torque control can better suppress torque ripple and obtain smoother rotation speed [10]. This article focuses its research on MPTC.

Actually, there has been much literature on MPTC. Ref. [11] proposes double-vector control, which selects an effective voltage vector and a zero-voltage vector in one control cycle to reduce torque ripple. Ref. [12] proposes generalized double-vector control, which extends the second vector of double-vector control from zero-vector to an arbitrary voltage vector, and experiments show that the system has a better effect. Ref. [13] proposes three-vector control, which can select three different voltage vectors in one control cycle. But limited by the computing power of the controller, the third voltage vector can only be a zero-vector, which shows that the three-vector control requires a lot of computation. Refs. [14–16] are all based on the three-vector control. Ref. [14] extends the candidate voltage vector to any direction and any amplitude. Ref. [15] uses a load observer to observe the load torque change, and feed-forward compensation is used to improve the dynamic response of the system. Ref. [16] adopts the delay compensation control to reduce the action delay caused by the calculation. The multi-vector control can improve the steady-state characteristics, but the increase of the computational amount brought by it is unavoidable, which makes the control process more complicated. The voltage vector

*Received 9 June 2022, Accepted 7 August 2022, Scheduled 26 August 2022*
* Corresponding author: Yang Zhang (459387623@qq.com).
[1] College of Electrical and Information Engineering, Hunan University of Technology, Zhuzhou 412007, China. [2] China Railway Signal and Communication (Changsha) Railway Traffic Control Technology Co. Ltd, Changsha 410000, China.

determination scheme based on the deadbeat principle used in [17, 18] only needs to calculate once to obtain the optimal voltage vector. This idea appeared earlier in continuous control set-MPC: predict the optimal output state of the inverter at the next moment according to the demand of the control system, and then use space vector pulse width modulation (SVPWM) or other modulation methods to achieve this optimal predicted value. The approach of [17, 18] is to predict the optimal inverter voltage vector once and then find a basic voltage output that is closest to the optimal vector. This method only needs to predict once. However, his prediction formula is very complex and requires high parameter accuracy. The overall computational effort is not well improved. Also, there is an inherent error in using the closest base voltage to replace the optimum voltage.

The subdivision sector vector is an emerging research direction nowadays. Ref. [19] subdivides the sector into twelve and synthesized six basic voltage vectors in pairs to obtain twelve effective voltage vectors, which reduced steady-state torque ripple and improved torque and flux smoothness. However, it requires 13 predictions in one control cycle, which greatly increases the amount of computation. Ref. [20] uses a torque hysteresis controller to select candidate voltage vectors from 12 voltage vectors, which reduces the computational cost, but the candidate voltage vectors obtained from torque and flux errors may not be completely suitable, depending on Motor speed and actual torque. Ref. [21] proposes a virtual voltage vector construction scheme. The new virtual voltage vector consists of adjacent base voltage vectors. The purpose of adding the zero voltage vector in [21] is to make the voltage vector amplitude adjustable. The duty cycle control method needs to involve calculating the action time of the effective voltage vector and zero voltage vector. This approach is not conducive to further reducing the computational burden.

Aiming at computational cost and torque fluctuation, this paper proposes a fast predictive switching table on the basis of sector division, which not only reduces the amount of calculation but also improves the steady-state characteristics of the system. In addition, the weight coefficient PI controller about the load torque is designed, and the weight coefficient could be adjusted with the torque to improve the dynamic characteristics of the system.

## 2. MPTC OF PMSM

### 2.1. Mathematical Model of PMSM

Under the $dq$ rotating coordinate axis system, the mathematical model of the permanent magnet synchronous motor is as follows [22]. The stator voltage equation is

$$\begin{cases} U_d = R_s i_d + \dfrac{d\psi_d}{dt} - \omega_r \psi_q \\ U_q = R_s i_q + \dfrac{d\psi_q}{dt} + \omega_r \psi_d \end{cases} \tag{1}$$

The flux linkage equation is

$$\begin{cases} \psi_d = L_d i_d + \psi_f \\ \psi_q = L_q i_q \end{cases} \tag{2}$$

The electromagnetic torque equation is

$$T_e = \frac{3}{2} p_n \left(\psi_s \otimes i_s\right) = \frac{3}{2} p_n \left(\psi_d i_q - \psi_q i_d\right) = \frac{3}{2} p_n \left[\psi_f i_q + \left(L_d - L_q\right) i_d i_q\right] \tag{3}$$

By substituting Equation (2) into (1), the stator voltage equation can also be expressed as

$$\begin{cases} U_d = R_s i_d + L_d \dfrac{di_d}{dt} + \omega_r L_q i_q \\ U_q = R_s i_q + L_q \dfrac{di_q}{dt} + \omega_r L_d i_d + \omega_r \psi_f \end{cases} \tag{4}$$

where $U_d$, $U_q$, $i_d$, $i_q$, $\psi_d$, $\psi_q$ respectively are the direct-axis and quadrature-axis stator voltages, stator currents, and stator flux linkages. $\psi_s$ is the stator flux linkage; $\psi_f$ is the permanent magnet flux linkage; $R_s$ is the resistance of the three-phase stator winding; $p_n$ is the number of pole pairs; $\omega_r$ is

the electrical angular velocity. The inductance value of surface-mount permanent magnet synchronous motor (SPMSM) is $L_d = L_q = L_s$. The electromagnetic torque, in this case, can be simplified as

$$T_e = \frac{3}{2} p_n \psi_f i_q \tag{5}$$

### 2.2. Traditional MPTC

The control strategy of the traditional MPTC uses a three-phase voltage-type inverter to drive the PMSM and performs real-time predictions from 7 switching states to obtain 7 predicted torques and predicted flux linkages. After that, it uses the principle of minimum cost function to select the most suitable candidate voltage vector and the corresponding switching state, so as to control the inverter output for the desired switching state.

From Equations (6) and (7), the $dq$-axis voltage applied to the motor under all predicted switching states can be obtained.

$$\begin{cases} U_A = \dfrac{1}{3} U_{dc} \left(2S_a - S_b - S_c\right) \\ U_B = \dfrac{1}{3} U_{dc} \left(2S_b - S_a - S_c\right) \\ U_C = \dfrac{1}{3} U_{dc} \left(2S_c - S_a - S_b\right) \end{cases} \tag{6}$$

$$\begin{cases} U_d = \dfrac{2}{3} \left[U_A \cos\theta + U_B \cos\left(\theta - \frac{2}{3}\pi\right) + U_C \cos\left(\theta + \dfrac{2}{3}\pi\right)\right] \\ U_q = \dfrac{2}{3} \left[U_A \sin\theta + U_B \sin\left(\theta - \frac{2}{3}\pi\right) + U_C \sin\left(\theta + \dfrac{2}{3}\pi\right)\right] \end{cases} \tag{7}$$

The current differential is derived from Equation (4) as

$$\begin{cases} \dfrac{di_d}{dt} = \dfrac{1}{L_s}[U_d - R_s i_d - \omega_r L_s i_q] \\ \dfrac{di_q}{dt} = \dfrac{1}{L_s}[U_q - R_s i_q - \omega_r L_s i_d - \omega_r \psi_f] \end{cases} \tag{8}$$

Using the forward Euler method to discretize Equation (8), the predicted current at the next moment is derived as

$$\begin{cases} i_d^p(k+1) = (1 - \dfrac{R_s}{L_s} T_s) i_d(k) + T_s \omega_r i_q(k) + \dfrac{T_s}{L_s} U_d(k) \\ i_q^p(k+1) = (1 - \dfrac{R_s}{L_s} T_s) i_q(k) + T_s \omega_r i_d(k) - \dfrac{T_s}{L_s} \psi_f \omega_r + \dfrac{T_s}{L_s} U_q(k) \end{cases} \tag{9}$$

Combined with formulas (2), (5), and (9), it is derived that the predicted values of the flux linkage and torque at the next moment are

$$\begin{cases} \psi_d^p(k+1) = L_d i_d^p(k+1) + \psi_f \\ \psi_q^p(k+1) = L_q i_q^p(k+1) \\ \psi_s^p(k+1) = \sqrt{\psi_d^p(k+1)^2 + \psi_q^p(k+1)^2} \end{cases} \tag{10}$$

$$T_e^p(k+1) = \frac{3}{2} p_n \psi_f i_q^p(k+1) \tag{11}$$

Then a voltage vector is selected according to the principle of minimum cost function. The cost function expression is as follows

$$g = \lambda \left|T_e^* - T_s^p(k+1)\right| + \left|\psi_s^* - \psi_s^p(k+1)\right| \tag{12}$$

In the above formula, $S_a$, $S_b$, $S_c$ are the switching states of the three-phase inverter; $U_{dc}$ is the DC bus voltage; $U_A$, $U_B$, $U_C$ are the stator three-phase voltage; $\theta$ is the rotor position angle. Fig. 1 is the

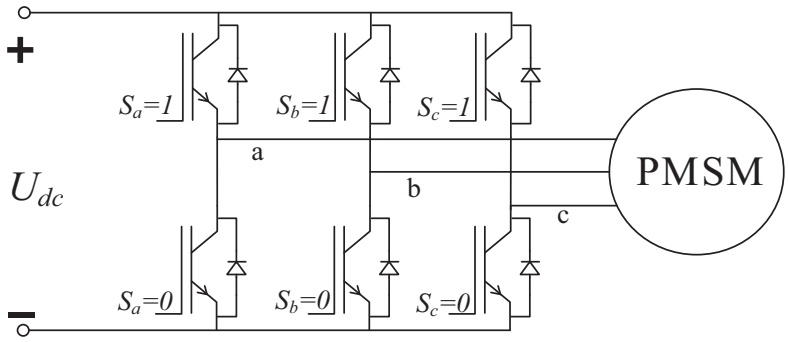


**Figure 1.** Schematic diagram of switching signal and inverter.

schematic diagram of the switching states and inverter. In it, $S_a = 1$ means that when the switch signal of phase $a$ is 1, the upper bridge arm of phase $a$ is turned on. Similarly, when $S_a = 0$, the lower bridge arm is turned on.

In the traditional MPTC, the weight coefficient generally uses the empirical value or selects $|\psi_s^*/T_e^*|$, so that the torque and flux linkage could be unitized.

## 3. FAST PREDICTIVE SWITCHING TABLE

### 3.1. Traditional Sector Division Model Predictive Torque Control

In order to improve the control effect of MPC and reduce the torque ripple, the sector division is introduced. Taking every 30° as a subdivided sector, the six basic voltage vectors are synthesized two by two into new voltage vectors. In this way, there are 6 basic voltage vectors, 6 synthetic voltage vectors, and 2 zero-voltage vectors. 14 vectors in total can be predicted.

With synthesizing the basic voltage vectors according to Equation (13), the six synthetic voltage vectors are obtained as follows

$$\begin{cases} U_2 = 0.1U_0 + 0.4U_1 + 0.4U_3 + 0.1U_{13} \\ U_4 = 0.1U_0 + 0.4U_3 + 0.4U_5 + 0.1U_{13} \\ U_6 = 0.1U_0 + 0.4U_5 + 0.4U_7 + 0.1U_{13} \\ U_8 = 0.1U_0 + 0.4U_7 + 0.4U_9 + 0.1U_{13} \\ U_{10} = 0.1U_0 + 0.4U_9 + 0.4U_{11} + 0.1U_{13} \\ U_{12} = 0.1U_0 + 0.4U_{11} + 0.4U_1 + 0.1U_{13} \end{cases} \tag{13}$$

As shown in Fig. 2, $U_1$, $U_3$, $U_5$, $U_7$, $U_9$, $U_{11}$ are six basic voltage vectors; $U_2$, $U_4$, $U_6$, $U_8$, $U_{10}$, $U_{12}$ are six synthetic voltage vectors; $U_0$, $U_{13}$ are zero-voltage vectors. Since a zero-voltage vector is added to the synthesis, the amplitude of the synthetic voltage vector is smaller than that of the basic voltage vector. Whereas, using fourteen voltage-vectors to predict will directly increase the prediction time by 6 times. Compared with the sampling time, if the computational time is longer, there will be a serious delay phenomenon, which may lead to the deterioration of the system performance, and it is not suitable for the occasions where the control time is required.

### 3.2. Fast Predictive Switching Table Based on Sector Division

In order to reduce the calculation amount and save the time of prediction, this paper proposes a fast predictive switching table on the basis of sector division. Referring to the controlling idea of DTC, all non-zero voltage vectors are divided into four types: increase torque with increasing flux linkage, increase torque with decreasing flux linkage, decrease torque with increasing flux linkage, and decrease torque with decreasing flux linkage.

As shown in Fig. 3, it is assumed that the motor rotates counterclockwise. Taking sector S1 as an example, the vectors are divided into four categories: the included angle with the stator flux linkage

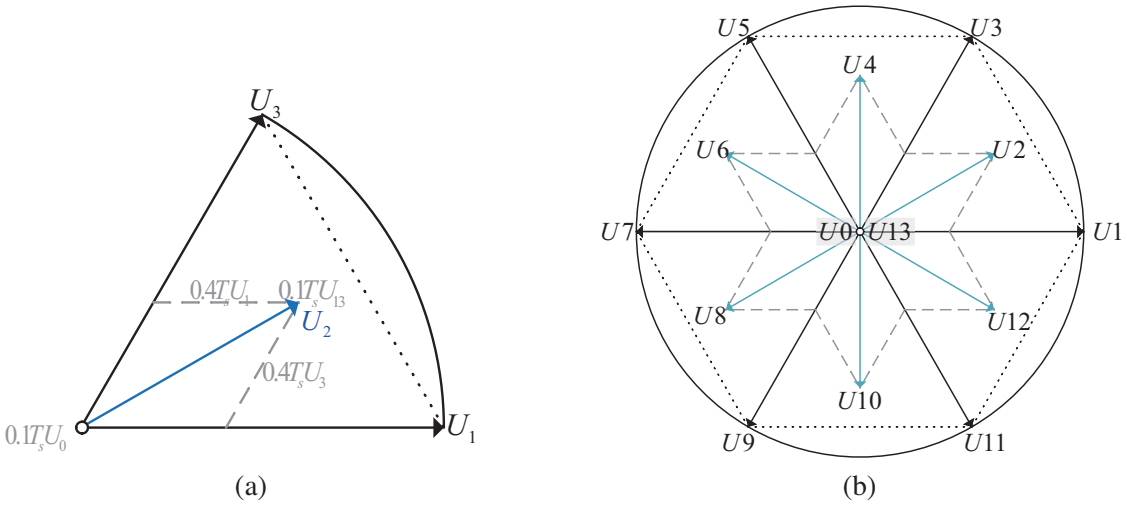


**Figure 2.** Synthesis of Voltage Vectors. (a) The way of voltage vector synthesis. (b) 12 voltage vectors for sector division.

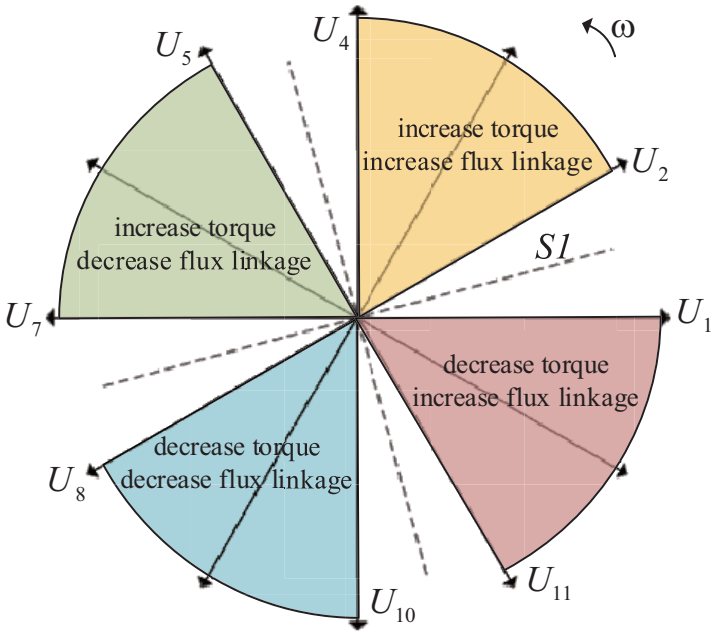


**Figure 3.** Analysis of the torque effect of sector S1.

between ($0° \sim 90°$) is represented by increasing torque and increasing flux linkage; the included angle between ($90° \sim 180°$) is represented by increasing torque and decreasing flux linkage; the included angle between ($180° \sim 270°$) is represented by decreasing torque and decreasing flux linkage; the included angle between ($270° \sim 360°$) is represented by decreasing torque and increasing flux linkage.

For SPMSM, the electromagnetic torque can also be expressed as

$$T_e = \frac{3}{2}\frac{p_n\,|\psi_s|}{L_d}\,(\psi_f \sin\delta) \tag{14}$$

Or in the incremental form

$$\Delta T_e = \frac{3}{2}\frac{p_n}{L_d}\psi_f\,(\Delta\psi_s \sin\delta + |\psi_s|\,\Delta\delta\cos\delta) \tag{15}$$

It can be seen from Equation (15) that the torque increment depends on the increment of the stator flux linkage amplitude $|\psi_s|$ and the stator flux linkage angle $\delta$. In the case of ignoring the voltage drop of the stator resistance, the relationship between the voltage vector $\vec{U}_s$ and flux linkage vector $\vec{\psi}_s$ can be expressed as

$$\Delta\overrightarrow{\psi_s} = \overrightarrow{U_s}\Delta t \tag{16}$$

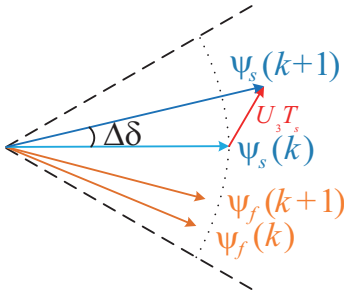


**Figure 4.** The flux linkage changes under the action of voltage.

As shown in Fig. 4, when the angle between the applied stator voltage and stator flux linkage is 90°, the increased torque is the largest; when the angle between the applied stator voltage and the stator flux linkage is −90°, the reduced torque is the largest [23]. Also taking sector S1 as an example, the goal is to reduce the pulsation of steady-state torque. In this way, the switching table selects vector U2 in the sector that increases torque and increases flux linkage; selects vector U7 in the sector that increases torque and reduces flux linkage; selects vector U8 in the sector that reduces torque and reduces flux linkage; selects vector U1 in the sector that reduces torque and increases flux linkage. The number of candidate voltage vectors of each sector is screened from 13 to 5 like that. In other words, the amount of computation is reduced by 61.54%. Table 1 is the fast predictive switching table of each sector at steady state.

**Table 1.** The fast predictive switching table at steady state.

| Effective voltage vector | | | | | Zero-voltage vector |
|---|---|---|---|---|---|
| Flux ($\psi = 1$ means increase, $\psi = 0$ means decrease) | $\psi = 1$ | | $\psi = 0$ | | |
| Torque ($T = 1$ means increase, $T = 0$ means decrease) | $T = 1$ | $T = 0$ | $T = 1$ | $T = 0$ | |
| $S1$ | $U_2$ | $U_1$ | $U_7$ | $U_8$ | $U$ |
| $S2$ | $U_3$ | $U_2$ | $U_8$ | $U_9$ | $U_{13}$ |
| $S3$ | $U_4$ | $U_3$ | $U_9$ | $U_{10}$ | $U_{13}$ |
| $S4$ | $U_5$ | $U_4$ | $U_{10}$ | $U_{11}$ | $U$ |
| $S5$ | $U_6$ | $U_5$ | $U_{11}$ | $U_{12}$ | $U$ |
| $S6$ | $U_7$ | $U_6$ | $U_{12}$ | $U_1$ | $U_{13}$ |
| $S7$ | $U_8$ | $U_7$ | $U_1$ | $U_2$ | $U_{13}$ |
| $S8$ | $U_9$ | $U_8$ | $U_2$ | $U_3$ | $U$ |
| $S9$ | $U_{10}$ | $U_9$ | $U_3$ | $U_4$ | $U$ |
| $S10$ | $U_{11}$ | $U_{10}$ | $U_4$ | $U_5$ | $U_{13}$ |
| $S11$ | $U_{12}$ | $U_{11}$ | $U_5$ | $U_6$ | $U_{13}$ |
| $S12$ | $U_1$ | $U_{12}$ | $U_6$ | $U_7$ | $U$ |

It should be pointed out that the candidate voltage vectors of each sector strictly follow the principle of reducing torque ripple. Ref. [24] proposes to use zero-vector to reduce the influence of "intermittently pulsating space voltage vector" on torque ripple. The zero-vector plays a very important role in reducing the torque ripple, so it is necessary to add the zero-vector to the switching table, which is also a particularly critical reason for adding the zero-vector to the vector synthesis. The selection principle of the zero-vector is to select one with the minimum switching times. Each control process is predicted only 5 times, compared with 13 predictions for traditional sector division control, which reduces a lot of calculations, and there are also zero-vectors added to the effective vector, which make the torque and flux linkage smoother at the steady state. The target voltage output by the inverter is selected from the candidate voltage vectors in the table according to the principle of minimum cost function and acts for a whole control cycle. The action time of the synthetic voltage vector is determined according to Equation (13), and the application of the zero vector follows the minimum switching times. For example, using the voltage vector U2, the voltage vector U0 $(0,0,0)$ acts for 0.1 times of the control period Ts; U1 $(1,0,0)$ acts for 0.4 times of Ts; U3 $(1,1,0)$ acts for 0.4 times Ts; U13 $(1,1,1)$ acts for 0.1 times of Ts. The selected voltage vector is converted into the corresponding switching state by the pulse generator.

## 4. DYNAMIC PERFORMANCE IMPROVEMENTS

### 4.1. The Fast Predictive Switching Table at Dynamic State

In order to improve the dynamic response speed of PMSM, this paper proposes the dynamic fast predictive switching table and dynamically adjustable weight coefficient. When the motor is just started, the motor torque is far lower than the rated torque, and the candidate voltage of MPTC is changed from the predictive switching table at steady state to the predictive switching table at dynamic state. Actually, the predictive switching table at dynamic state is based on the predictive switching table at steady state, with an improvement in terms of increasing torque. The primary goal of the predicted voltage vector is to increase the torque so as to shorten the time for the torque to reach the rated value, thereby improving the dynamic characteristics of the motor. If it is set to switch to the dynamic switch table when the actual torque value is lower than 50% of the rated torque value, the shortened time is not obvious, because, in fact, the torque spends less time in the early stage of rising. Besides, the load disturbance also needs to be considered, so this paper sets that when the actual torque value is lower than 80% of the rated torque value, it is switched to the dynamic fast predictive switch table. Next, the paper describes how the dynamic fast predictive switching table is improved.

According to Equation (11), the differential form of torque can be expressed as

$$\frac{dT_e^p(k+1)}{dt} = \frac{3}{2} p_n \psi_f \frac{di_q^p(k+1)}{dt} \tag{17}$$

From Equation (16), the torque differential is proportional to the stator current differential, and the $q$-axis stator current differential formula is expressed as

$$\frac{di_q^p(k+1)}{dt} = \frac{1}{L_s}\left[u_q^p(k+1) - A\right] \tag{18}$$

In the formula, $A = R_s i_q(k) + \omega_r L_s i_d(k) + \omega_r \psi_f$. If the influence of the last predicted value is ignored, focusing on the torque increased at the moment $(k+1)$, it can be found that the differential of the $q$-axis stator current is proportional to the $q$-axis stator voltage. The $q$-axis stator voltage at the time $(k+1)$ is expressed as

$$u_q^p(k+1) = -u_\alpha^p(k+1)\sin\theta + u_\beta^p(k+1)\cos\theta \tag{19}$$

The relationship between the 14 candidate voltage vectors after Clark transformation and the predicted value of $u_q^p(k+1)$ can be shown in Fig. 5.

Combining Fig. 5 and the above theory, selecting a candidate voltage vector with the largest $u_q^p(k+1)$ value can increase the torque the most. Taking the S1 sector as an example, the following conclusions can be clearly seen in Fig. 3 and Fig. 5. The best choice that meets torque and the flux linkage increase requirements is the U3 vector; the best choice that meets the torque increase and flux

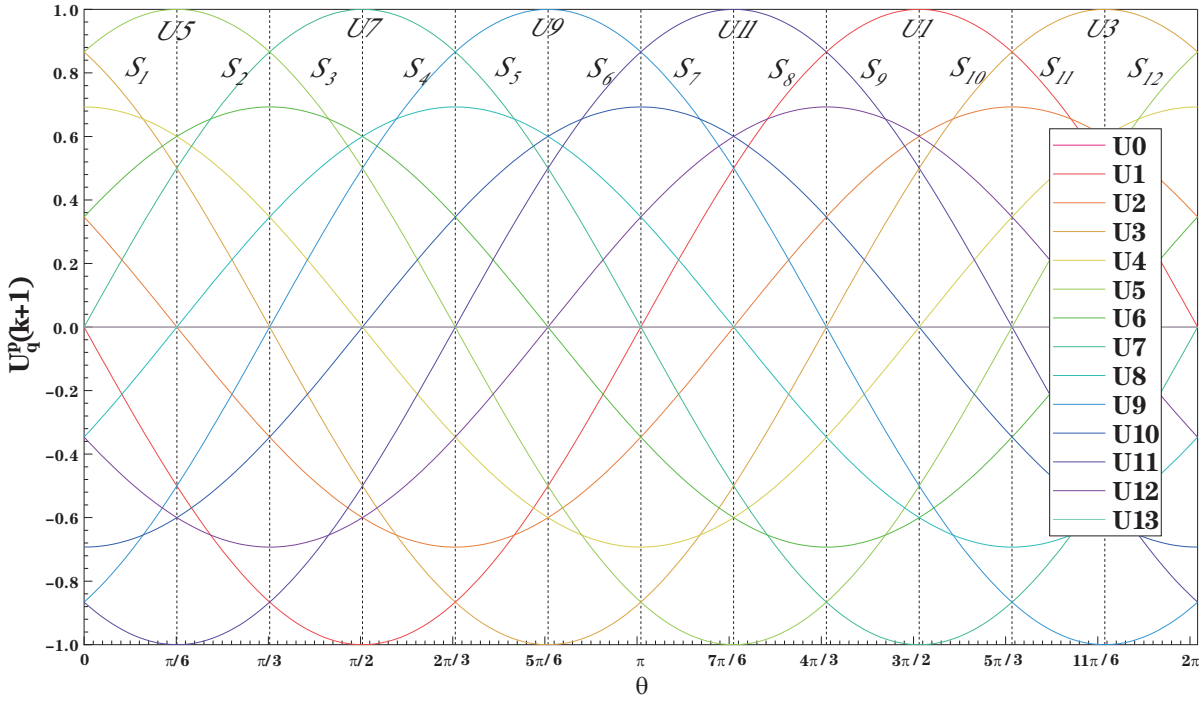


**Figure 5.** The relationship between candidate voltage vectors and predicted $q$-axis voltage $u_q^p(k+1)$ in all sector.

linkage reduction requirements is the U5 vector. Therefore, referring to the data in Fig. 5, the fast predictive switching table for increasing torque with improved dynamic characteristics is obtained, as shown in Table 2.

**Table 2.** The fast predictive switching table for increased torque at dynamic state.

| Effective voltage vector | | | | | Zero-voltage vector |
|---|---|---|---|---|---|
| Flux ($\psi = 1$ means increase, $\psi = 0$ means decrease) | $\psi = 1$ | | $\psi = 0$ | | |
| Torque ($T = 1$ means increase, $T = 0$ means decrease) | $T = 1$ | $T = 0$ | $T = 1$ | $T = 0$ | |
| $S1$ | $U_3$ | $U_1$ | $U_5$ | $U_8$ | $U$ |
| $S2$ | $U_5$ | $U_2$ | $U_7$ | $U_9$ | $U_{13}$ |
| $S3$ | $U_5$ | $U_3$ | $U_7$ | $U_{10}$ | $U_{13}$ |
| $S4$ | $U_7$ | $U_4$ | $U_9$ | $U_{11}$ | $U$ |
| $S5$ | $U_7$ | $U_5$ | $U_9$ | $U_{12}$ | $U$ |
| $S6$ | $U_9$ | $U_6$ | $U_{11}$ | $U_1$ | $U_{13}$ |
| $S7$ | $U_9$ | $U_7$ | $U_{11}$ | $U_2$ | $U_{13}$ |
| $S8$ | $U_{11}$ | $U_8$ | $U_1$ | $U_3$ | $U$ |
| $S9$ | $U_{11}$ | $U_9$ | $U_1$ | $U_4$ | $U$ |
| $S10$ | $U_1$ | $U_{10}$ | $U_3$ | $U_5$ | $U_{13}$ |
| $S11$ | $U_1$ | $U_{11}$ | $U_3$ | $U_6$ | $U_{13}$ |
| $S12$ | $U_3$ | $U_{12}$ | $U_7$ | $U_7$ | $U$ |

Similarly, after adjusting the voltage vector that reduces torque, the fast predictive switching table for decreasing torque with improved dynamic characteristics is obtained, as shown in Table 3.

**Table 3.** The fast predictive switching table for decreasing torque at dynamic state.

| Effective voltage vector | | | | | Zero-voltage vector |
|---|---|---|---|---|---|
| Flux ($\psi = 1$ means increase, $\psi = 0$ means decrease) | $\psi = 1$ | | $\psi = 0$ | | |
| Torque ($T = 1$ means increase, $T = 0$ means decrease) | $T = 1$ | $T = 0$ | $T = 1$ | $T = 0$ | |
| $S1$ | $U_2$ | $U_{11}$ | $U_7$ | $U_9$ | $U$ |
| $S2$ | $U_3$ | $U_1$ | $U_8$ | $U_{11}$ | $U_{13}$ |
| $S3$ | $U_4$ | $U_1$ | $U_9$ | $U_{11}$ | $U_{13}$ |
| $S4$ | $U_5$ | $U_3$ | $U_{10}$ | $U_1$ | $U$ |
| $S5$ | $U_6$ | $U_3$ | $U_{11}$ | $U_1$ | $U$ |
| $S6$ | $U_7$ | $U_5$ | $U_{12}$ | $U_3$ | $U_{13}$ |
| $S7$ | $U_8$ | $U_5$ | $U_1$ | $U_3$ | $U_{13}$ |
| $S8$ | $U_9$ | $U_7$ | $U_2$ | $U_5$ | $U$ |
| $S9$ | $U_{10}$ | $U_7$ | $U_3$ | $U_5$ | $U$ |
| $S10$ | $U_{11}$ | $U_9$ | $U_4$ | $U_7$ | $U_{13}$ |
| $S11$ | $U_{12}$ | $U_9$ | $U_5$ | $U_7$ | $U_{13}$ |
| $S12$ | $U_1$ | $U_{11}$ | $U_6$ | $U_9$ | $U$ |

### 4.2. Dynamically Adjusted Weight Coefficients

The weight coefficient of MPTC is also an important factor affecting torque rise, thus the PI-besed dynamic adjusted weight coefficient is designed in this paper, as shown in Fig. 6. Its process is that firstly system estimates the torque at the current moment according to Equation (11). Then it calculates the difference between the actual torque and the given torque at the current moment, and after the proportional-integral controller and limiter, its output is a weight coefficient $\lambda$. Obviously, the weight coefficient $\lambda$ varies with the torque change. The design principles of the weight coefficient PI controller are: (1) In order to have a faster response time, $K_p$ should not be too small; (2) $K_i$ should be as small as possible, but it can eliminate the residual error; (3) A limiter is added to the output, and the limit value is the most stable value of the current system weight factor.

When the torque difference is larger, the PI controller outputs a larger weight coefficient. According to Equation (12), the increase of the value of $\lambda$ makes the cost function pay more attention to the torque

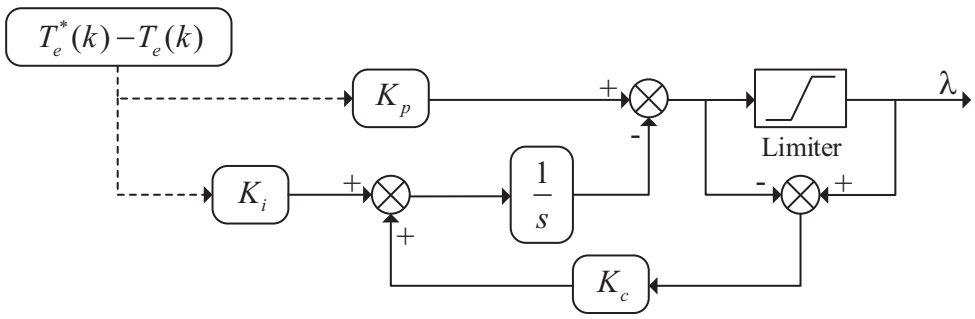


**Figure 6.** The weight coefficient PI controller.

for following the given value in the calculation, and the property that $\lambda$ can be adjusted also increases the robustness of the system. Since there is no corresponding calculation formula for the weight coefficient, it is obtained through empirical experiments in most articles. The stable value of the weight coefficient in this paper is 1/55.

The structural block diagram of the PMSM system is shown in Fig. 7. In the figure, the speed outer loop adopts PI control. The current inner loop performs sector judgment according to the inverter voltage, and then uses the fast predicative switching table-based MPTC. The flux linkage calculation adopts the control method of maximum torque per ampere (MTPA). The purpose of MTPA is to produce maximum torque with the minimum current. After calculating the current according to the torque, the flux linkage is further calculated. The weight coefficient PI controller is added to the inner loop. These constitute the fast predicative switching table-based MPTC control system with a weighted coefficient PI controller.

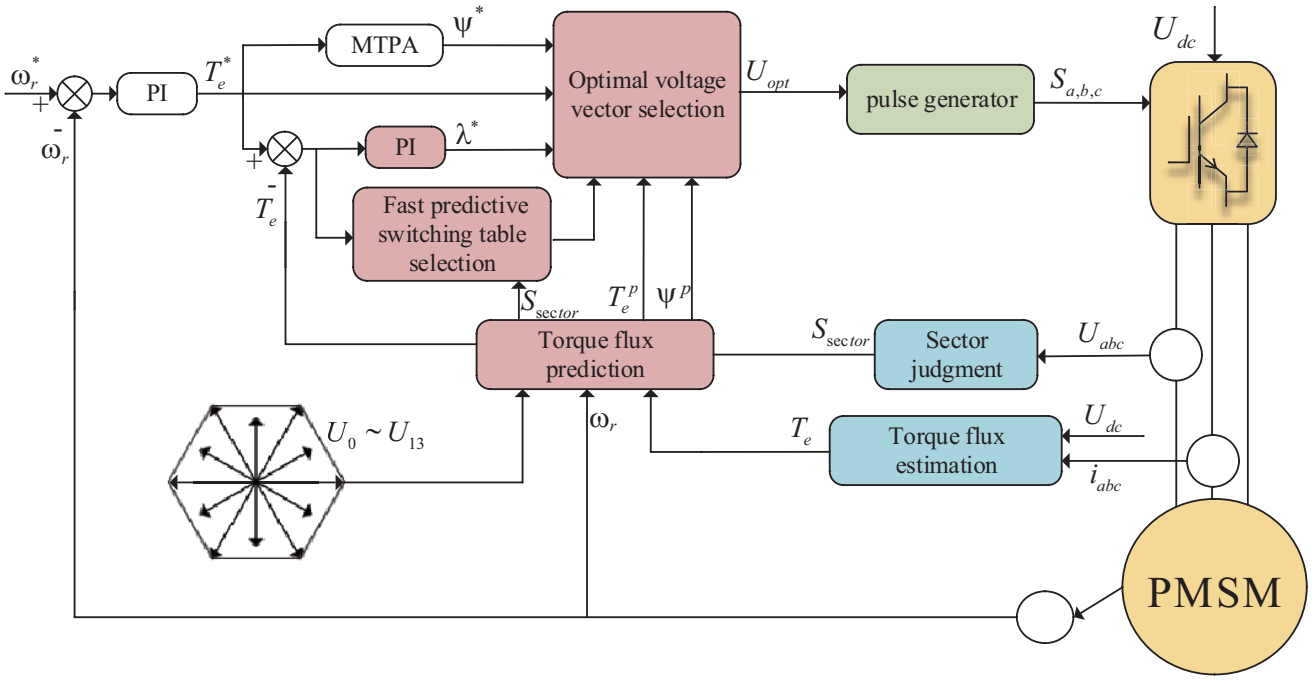


**Figure 7.** The structural block diagram of the fast predicative switching table-based MPTC control system with a weighted coefficient PI controller.

## 5. EXPERIMENTAL VERIFICATION

The following experiments are used to verify the validity of the conclusions of the proposed method. All experimental waveforms were generated by the RT-LAB experimental platform in Fig. 8. The RT-LAB hardware-in-the-loop system (HILS) configuration is shown in Fig. 9. In HILS, the Digital Signal Processor (DSP) model is TMS320F2812,, and other parts of the system such as PMSM and inverter are constructed with RT-LAB (op5600).

The experiment uses SPMSM, and the specific parameters are shown in Table 4. To better observe the control effect on the oscilloscope, the output of speed and torque are multiplied by a certain coefficient, the speed coefficient $k_n$ is 1/151, and the torque coefficient $k_{T_e}$ is 1.5. In addition, the speed loop uses the same PI parameters to avoid the influence of its PI parameters on the system performance.

In the experiment, the SPMSM started with no-load at 0.0 s, and its speed reached 1200 rpm; at 0.15 s, a load of 3 N m was suddenly added; at 0.2 s, its speed increased to 1500 rpm; at 0.3 s, it was unloaded. Fig. 10 shows the speed experimental waveforms of traditional MPTC, the sector division

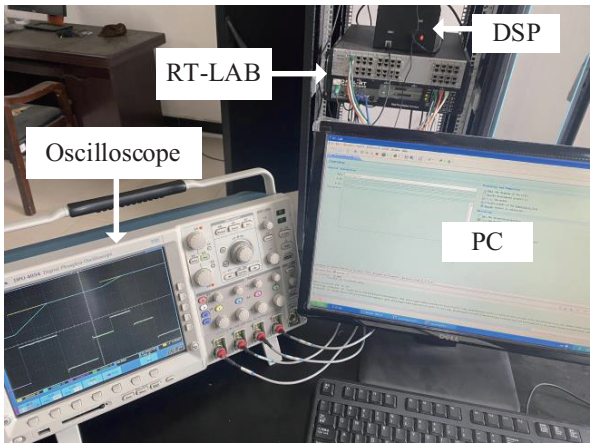


**Figure 8.** RT-LAB experiment platform.

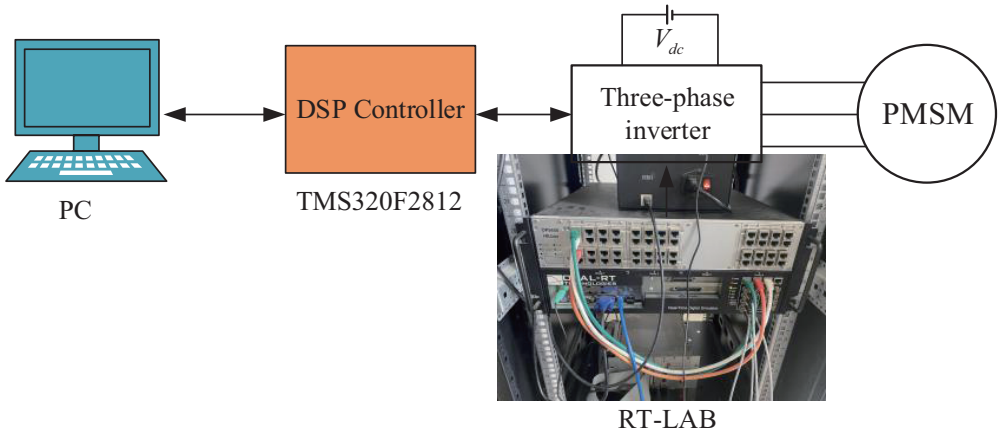


**Figure 9.** RT-LAB hardware-in-the-loop system configuration.

**Table 4.** Motor parameter.

| Parameter | Value | Unit |
|---|---|---|
| Number of pole pairs | 4 | pairs |
| Permanent magnet flux ($\psi_f$) | 0.1227 | Wb |
| Stator inductance ($L_s$) | 5.65 | mH |
| Stator resistance ($R_s$) | 1.35 | Ω |
| Rated torque ($T_N$) | 5 | Nm |
| Rated speed ($N$) | 1500 | r/min |
| Inertia ($J$) | 0.00315 | $\mathrm{kg \cdot m^2}$ |

MPTC, and the fast predicative switching table-based MPTC. It can be seen from the figure that the speed response of the three control methods is relatively rapid. When the load suddenly changes, all three control strategies can achieve smooth and fast speed tracking without overshoot. The fast predicative switching table-based MPTC reduces the number of voltage candidate vectors from 14 to 5, thus reducing the computational burden of the system. From the analysis of the experimental results, the improvement of the algorithm does not affect the speed response of the predictive control.

Figure 11 shows the torque waveforms of the three control strategies when the motor is loaded and unloaded. It is not difficult to see from the figure that sector division has a suppressing effect on torque

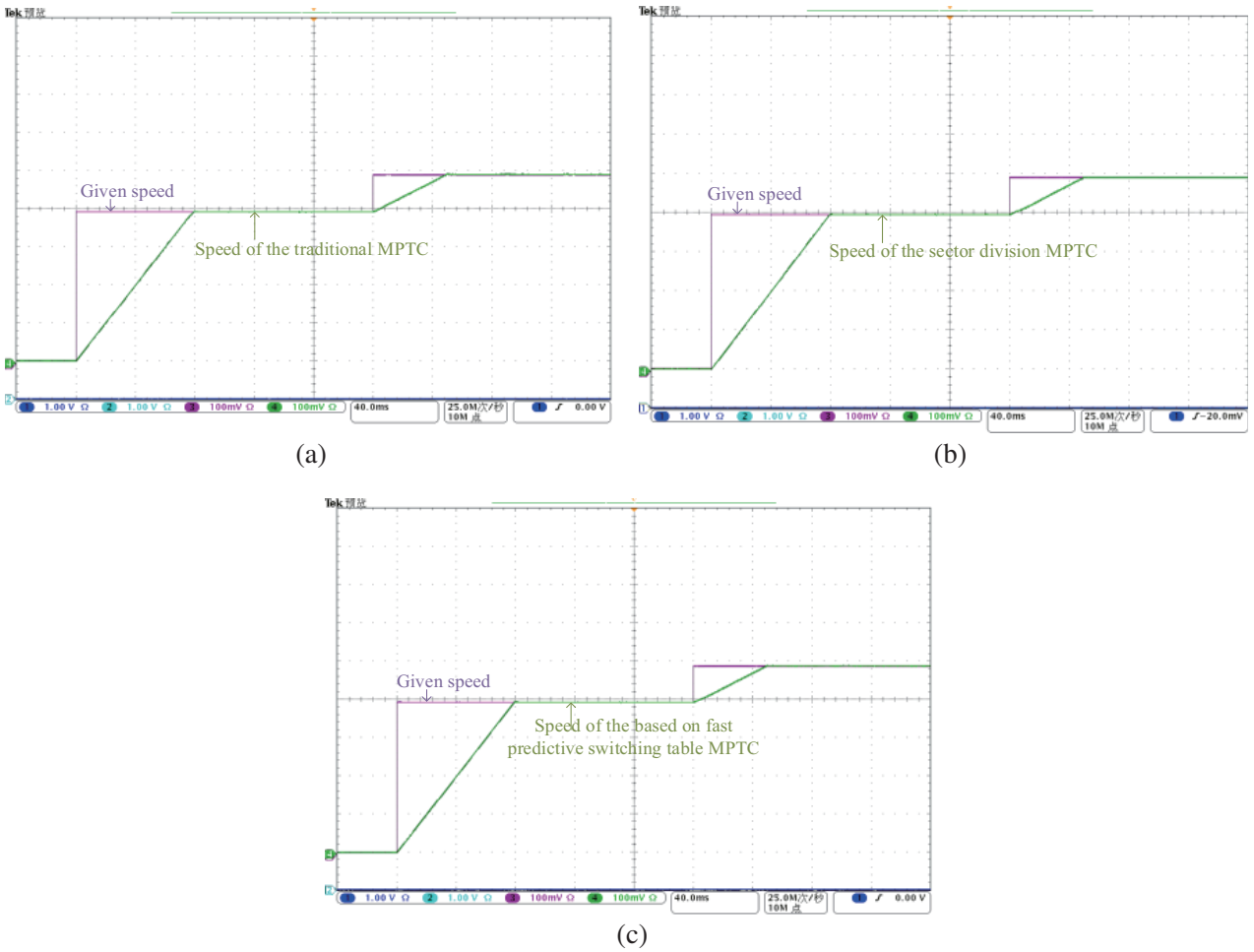


**Figure 10.** Experimental waveforms of rotational speed with different control methods. (a) The traditional MPTC. (b) The sector division MPTC. (c) the fast predicative switching table-based MPTC.

ripple. At steady state, the torque fluctuation range of the traditional MPTC is 2.79 $\sim$ 3.17 Nm; the torque fluctuation range of the sector division MPTC is 2.85 $\sim$ 3.05 Nm; the torque fluctuation range of the fast predicative switching table-based MPTC is 2.86 $\sim$ 3.07 Nm. The detailed data are shown in Table 5. It is analyzed that the sector division MPTC reduces the torque ripple from 0.38 Nm to 0.2 Nm

**Table 5.** Torque comparison at steady state.

| Parameter | The traditional MPTC | The sector division MPTC | The fast predicative switching table-based MPTC |
|---|---|---|---|
| $T_{\text{emin}}$ (N · m) | 2.79 | 2.85 | 2.86 |
| $T_{\text{emax}}$ (N · m) | 3.17 | 3.05 | 3.07 |
| $\Delta T_{\text{emin}}$ (N · m) | 0.12 | 0.09 | 0.09 |
| $\Delta T_{\text{emax}}$ (N · m) | 0.38 | 0.20 | 0.21 |
| $\eta$ | 12.7% | 6.7% | 7% |

($T_{\text{emin}}$ is the minimum torque during loading; $T_{\text{emax}}$ is the maximum torque during loading; $\Delta T_{\text{emin}}$ is the minimum torque ripple during loading; $\Delta T_{\text{emax}}$ is the maximum torque ripple during loading; $\eta$ is the ratio of $\Delta T_{\text{emax}}$ to the load torque 3 Nm).

according to the data. Since the method proposed in this paper requires 61.54% less computation time than sector division MPTC, the steady-state torque ripple increases slightly. However, compared with the traditional MPTC, it can also effectively reduce the steady-state torque ripple by 0.21 Nm.

By adjusting the zoom knob of the oscilloscope, the dynamic characteristics of the torque when the motor is just started can be observed. Fig. 12 are experimental waveforms reflecting the dynamic characteristics of torque. From the information in the figure, the time represented by one grid distance is 100 µs. It can be seen that the torque increases to the rated value at 286 µs using the traditional MPTC control strategy. The sector division MPTC subdivides the basic 6 sectors into 12 sectors and uses multi-voltage vectors to predict. If this method is used, the time for the motor torque to reach the rated torque can be shortened to 267 µs. However, the shortened time is finite. After comparison, in the start-up stage, only the voltage vector selected by the fast predictive switching table is used, which takes less time than using all the voltage vectors. Time taken for torque to reach the rated value is reduced from 267 µs to 256 µs. The reason is that the cost function does not only care about the increase of torque when choosing the voltage vector, and the method proposed in this paper optimizes its selection. On the basis of fast predictive switching table, adding the weight coefficient PI controller will further improve the dynamic response. Using the fast predicative switching table-based MPTC with the weight coefficient PI controller, the time for torque to reach the rated value is 241 µs. Compared with the traditional MPTC, this time is reduced by 45 µs. The performance shows that the introduction of the controller is excellent for the dynamic characteristics of the system.

The experimental data are listed in Table 6, and it can be seen that the improved dynamic response

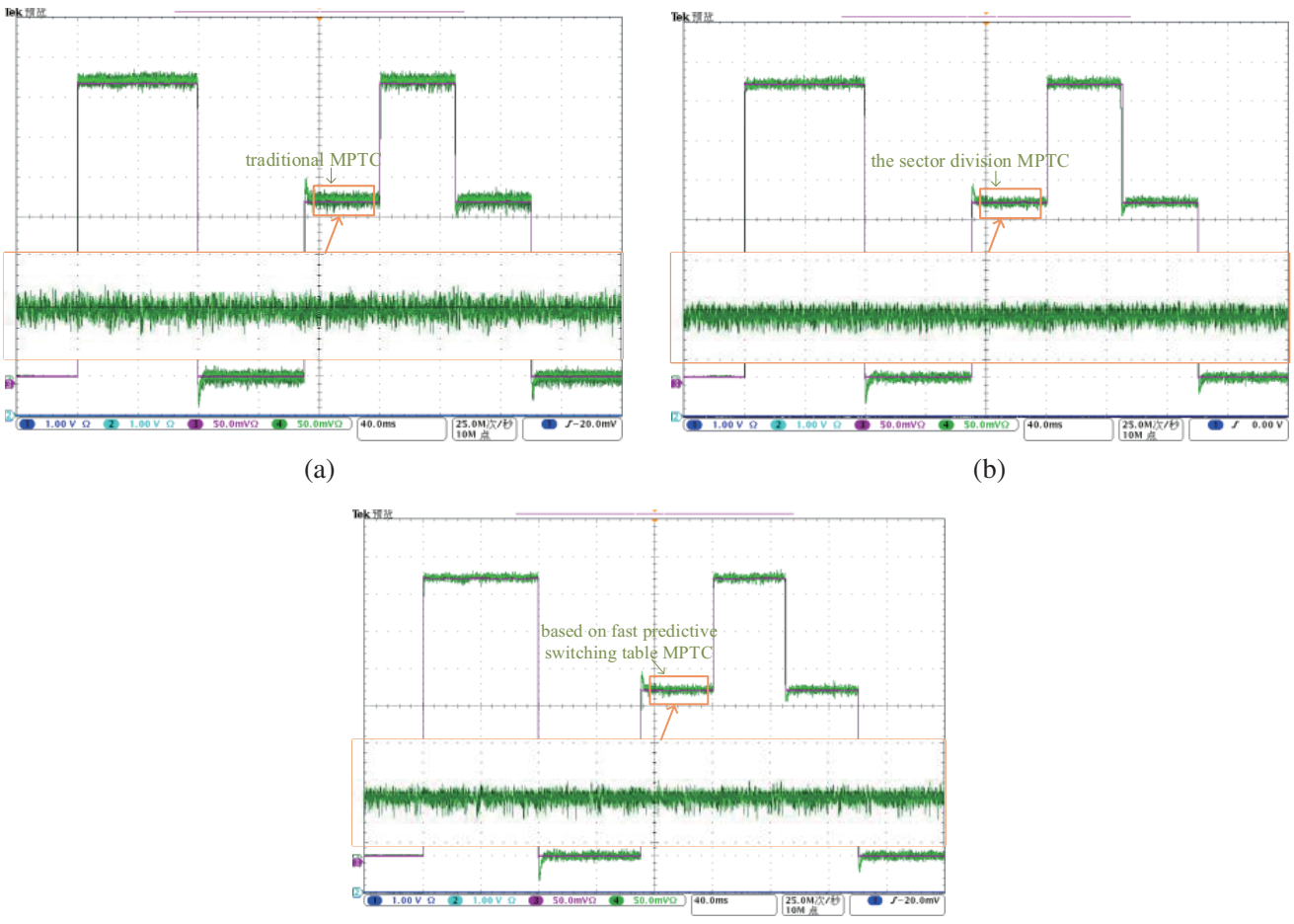


**Figure 11.** Experimental waveforms of torque with different control methods. (a) The traditional MPTC. (b) The sector division MPTC. (c) the fast predicative switching table-based MPTC.

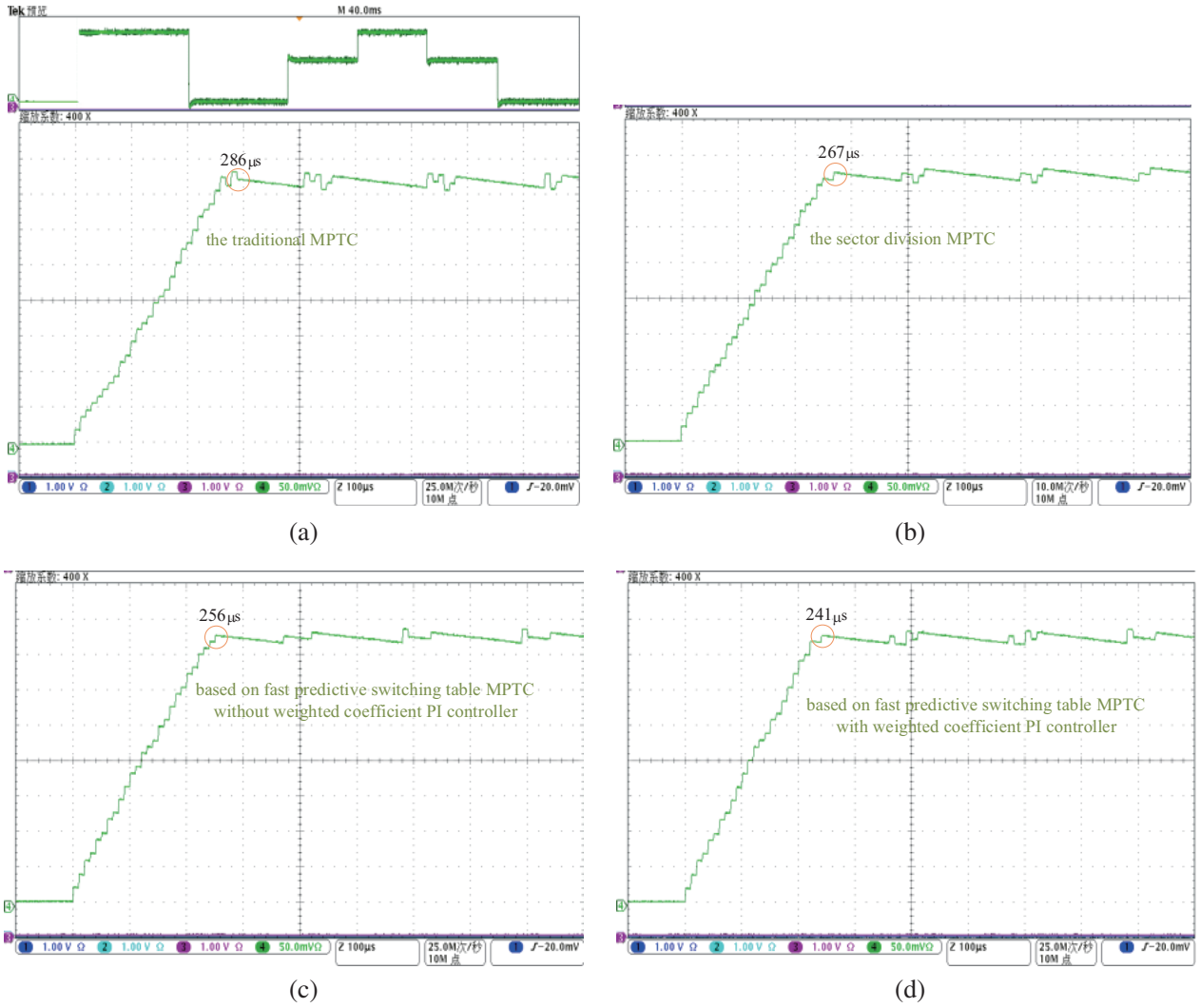


**Figure 12.** Experimental waveform of torque dynamic characteristics with different control methods. (a) The traditional MPTC. (b) The sector division MPTC. (c) The fast predicative switching table-based MPTC without the weight coefficient PI controller. (d) The fast predicative switching table-based MPTC with the weight coefficient PI controller.

**Table 6.** Torque comparison at dynamic.

| Parameter | The traditional MPTC | The sector division MPTC | The fast predicative switching table-based MPTC without the weight coefficient PI controller | The fast predicative switching table-based MPTC with the weight coefficient PI controller |
|---|---|---|---|---|
| $\Delta S$ (μs) | 286 | 267 | 256 | 241 |
| $\Delta T$ (μs) | | 19 | 30 | 45 |
| $\rho$ | 0% | 6.64% | 10.49% | 15.73% |

($\Delta S$ is the time for motor torque to reach rated torque; $\Delta T$ is the $\Delta S$ time difference between various methods and the traditional MPTC; $\rho$ is the ratio of $\Delta T$ to the time 286 μs used by the traditional MPTC).

method in this paper has been verified. Using the method proposed in this paper, the time for the motor torque to reach its rated value is only 84.26% of that of the traditional method. In some occasions where the torque is required to change rapidly, the time saving of 15.74% is undoubtedly valuable.

## 6. CONCLUSION

This paper analyzes the sector division MPTC control strategy and finds that its calculation process is complicated, and there is no weight coefficient design. In response to these problems, a method based on fast predictive switching table MPTC is proposed. The method uses specific vector combinations as candidate voltage vectors in each sector to reduce the computational complexity and combines these vector combinations into a switching table. The switch table ensures the control effect of the PMSM system under the condition that the computational time is reduced. At the same time, the weight coefficient PI controller is constructed, and the coefficient could be adjusted with motor torque. The following conclusions were drawn from the experiments: (1) Compared with the sector division MPTC, the fast predicative switching table-based MPTC reduces the computational cost, and the system has similar steady-state characteristics and better dynamic characteristics. (2) The weight coefficient PI controller improves the torque response speed while maintaining the torque stability. With the PI controller, the time for the torque to reach the rated value is reduced by 15 µs.

## ACKNOWLEDGMENT

This work was supported by the National Natural Science Foundation of China under Grant Number 51907061, Educational Commission of Hunan Province of China under Grant Number 21B0552.

## REFERENCES

1. Kiselev, A., G. R. Catuogno, A. Kuznietsov, and R. Leidhold, "Finite-control-set MPC for open-phase fault-tolerant control of PM synchronous motor drives," *IEEE Transactions on Industrial Electronics*, Vol. 67, No. 6, 4444–4452, June 2020.
2. Niu, S., Y. Luo, W. Fu, and X. Zhang, "Robust model predictive control for a three-phase PMSM motor with improved control precision," *IEEE Transactions on Industrial Electronics*, Vol. 68, No. 1, 838–849, January 2021.
3. Gong, C., Y. Hu, J. Gao, Y. Wang, and L. Yan, "An better delay-suppressed sliding-mode observer for sensor-controlled PMSM," *IEEE Transactions on Industrial Electronics*, Vol. 67, No. 7, 5913–5923, July 2020.
4. Zhong, L., M. F. Rahman, W. Y. Hu, and K. W. Lim, "Analysis of direct torque control in permanent magnet synchronous motor drives," *IEEE Transactions on Power Electronics*, Vol. 12, No. 3, 528–536, May 1997.
5. Carlet, P. G., A. Favato, S. Bolognani, and F. Dörfler, "Data-driven continuous-set predictive current control for synchronous motor drives," *IEEE Transactions on Power Electronics*, Vol. 37, No. 6, 6637–6646, June 2022.
6. Yin, Z., Q. Hou, Y. Zhang, and D. Yuan, "Sensorless finite control set model predictive speed control of induction motor using adaptive full-order observer," *2021 IEEE International Conference on Predictive Control of Electrical Drives and Power Electronics (PRECEDE)*, 364–369, 2021.
7. Ahmed, A. A., B. K. Koh, and Y. I. Lee, "A comparison of finite control set and continuous control set model predictive control schemes for speed control of induction motors," *IEEE Transactions on Industrial Informatics*, Vol. 14, No. 4, 1334–1346, April 2018.
8. Gao, J., C. Gong, W. Li, and J. Liu, "Novel compensation strategy for calculation delay of finite control set model predictive current control in PMSM," *IEEE Transactions on Industrial Electronics*, Vol. 67, No. 7, 5816–5819, July 2020.
9. Zhou, Z., C. Xia, Y. Yan, Z. Wang, and T. Shi, "Torque ripple minimization of predictive torque control for PMSM with extended control set," *IEEE Transactions on Industrial Electronics*, Vol. 64, No. 9, 6930–6939, September 2017.

10. Dan, H., P. Zeng, W. Xiong, M. Wen, M. Su, and M. Rivera, "Model predictive control-based direct torque control for matrix converter-fed induction motor with reduced torque ripple," *CES Transactions on Electrical Machines and Systems*, Vol. 5, No. 2, 90–99, June 2021.
11. Xu, Y. Y., Q. Qing, Y. Z. Lei, B. C. Zhang, and Y. Y. Li, "Improved duty cycle model predictive torque control method for permanent magnet synchronous motor," *Electric Drive*, Vol. 47, No. 05, 14–17+44, 2017.
12. Zhang, B. C., Y. Y. Xu, and Q. Zhou, "Based on generalized two-vector model predictive current control for PMSM," *Electric Drive*, Vol. 47, No. 03, 17–20, 2017.
13. Xu, Y. Y., J. B. Wang, B. C. Zhang, and Q. Zhou, "Three vector model predictive current control for permanent magnet synchronous motor," *Transactions of China Electrotechnical Society*, Vol. 33, No. 05, 980–988, 2018.
14. Wang, Z., X. Zhang, and Y. Guo, "Three-vector predictive current control for interior permanent magnet synchronous motor," *2021 IEEE International Conference on Predictive Control of Electrical Drives and Power Electronics (PRECEDE)*, 443–448, 2021.
15. Xiao, Q., Z. Li, B. Luo, T. Wang, D. Wen, and Y. Zhang, "Improved three vector model predictive torque control of PMSM," *Progress In Electromagnetics Research M*, Vol. 109, 217–229, 2022.
16. Gao, J., C. Gong, W. Li, and J. Liu, "Novel compensation strategy for calculation delay of finite control set model predictive current control in PMSM," *IEEE Transactions on Industrial Electronics*, Vol. 67, No. 7, 5816–5819, July 2020.
17. Sun, X., T. Li, Z. Zhu, G. Lei, Y. Guo, and J. Zhu, "Speed sensorless model predictive current control based on finite position set for PMSHM drives," *IEEE Transactions on Transportation Electrification*, Vol. 7, No. 4, 2743–2752, December 2021.
18. Sun, X., Y. Zhang, G. Lei, Y. Guo, and J. Zhu, "An improved deadbeat predictive stator flux control with reduced-order disturbance observer for in-wheel PMSMs," *IEEE/ASME Transactions on Mechatronics*, Vol. 27, No. 2, 690–700, April 2022.
19. Kim, S., J. Park, J. Bae, K. Cho, and D.-H. Lee, "An advanced multiple predictive direct torque control of PMSM using PWM and the 12 sectors," *2019 IEEE 6th International Conference on Industrial Engineering and Applications (ICIEA)*, 27–32, 2019.
20. Kim, S. J., J. Park, and D.-H. Lee, "A predictive DTC-PWM using 12 vectors for permanent magnet synchronous motor," *2019 10th International Conference on Power Electronics and ECCE Asia (ICPE 2019 — ECCE Asia)*, 2498–2504, 2019.
21. Sun, X., T. Li, M. Yao, G. Lei, Y. Guo, and J. Zhu, "Improved finite-control-set model predictive control with virtual vectors for PMSHM drives," *IEEE Transactions on Energy Conversion*, doi: 10.1109/TEC.2021.3138905.
22. Kim, H., J. Han, Y.-I. Lee, J.-H. Song, and K.-B. Lee, "Torque predictive control of permanent-magnet synchronous motor using duty ratio prediction," *2013 IEEE International Symposium on Industrial Electronics*, 1–5, 2013.
23. Li, X., Z. Xue, L. Zhang, and W. Hua, "A low-complexity three-vector-based model predictive torque control for SPMSM," *IEEE Transactions on Power Electronics*, Vol. 36, No. 11, 13002–13012, November 2021.
24. Tian, C. and Y. W. Hu, "Research on the theory and control scheme of direct torque control system of permanent magnet synchronous motor," *Transactions of China Electrotechnical Society*, Vol. 1, 7–11, 2002.